Experimental and theoretical near-edge x-ray-absorption fine-structure studies of NO^+

Rebecka Lindblad,[1,2,3,*] Ludvig Kjellsson,[4,5] Emiliano De Santis,[4] Vicente Zamudio-Bayer,[3] Bernd von Issendorff,[6] Stacey L. Sorensen,[2] J. Tobias Lau,[3,6] Weijie Hua,[7] Vincenzo Carravetta,[8] Jan-Erik Rubensson,[4] Hans Ågren,[4] and Rafael C. Couto[9,†]

[1]*Inorganic Chemistry, Department of Chemistry, Ångström Laboratory, Uppsala University, SE-75121 Uppsala, Sweden*
[2]*Department of Physics, Lund University, Box 118, S-22100 Lund, Sweden*
[3]*Abteilung für Hochempfindliche Röntgenspektroskopie, Helmholtz-Zentrum Berlin für Materialien und Energie, Albert-Einstein-Strasse 15, 12489 Berlin, Germany*
[4]*Department of Physics and Astronomy, Uppsala University, Box 516, SE-751 20 Uppsala, Sweden*
[5]*European XFEL GmbH, Holzkoppel 4, 22869 Schenefeld, Germany*
[6]*Physikalisches Institut, Albert-Ludwigs-Universität Freiburg, Hermann-Herder-Strasse 3, 79104 Freiburg, Germany*
[7]*MIIT Key Laboratory of Semiconductor Microstructure and Quantum Sensing, Department of Applied Physics, School of Science, Nanjing University of Science and Technology, Nanjing 210094, China*
[8]*IPCF-CNR, via Moruzzi 1, 56124 Pisa, Italy*
[9]*Division of Theoretical Chemistry and Biology, School of Chemistry, Biotechnology and Health, Royal Institute of Technology, SE-106 91 Stockholm, Sweden*

(Received 10 July 2022; accepted 3 October 2022; published 21 October 2022)

Experimental near-edge x-ray-absorption fine-structure (NEXAFS) spectra of the nitrosonium NO^+ ion are presented and theoretically analyzed. While neutral NO has an open shell, the cation is a closed-shell species, which for NEXAFS leads to the simplicity of a closed-shell spectrum. Compared to neutral NO, the electrons in the cation experience a stronger Coulomb potential, which introduces a shift of the ionization potential towards higher energies, a depletion of intensity in a large interval above the π^* resonance, and a shift of the σ^* resonance from the continuum to below the ionization threshold. NEXAFS features at the nitrogen and oxygen K edges of NO^+ are compared, as well as NEXAFS features at the nitrogen edges of the isoelectronic closed-shell species NO^+, N_2, and N_2H^+.

DOI: 10.1103/PhysRevA.106.042814

I. INTRODUCTION

Near-edge x-ray-absorption fine-structure (NEXAFS) spectroscopy has, over a long period of time, developed to a vitally important analytical tool for the characterization of molecules and molecular materials. Recent instrumental progress has made it possible to include molecular ions in the portfolio of applications [1–10]. Combined experimental and theoretical studies of N_2^+ [5] and CO^+ [6] cations indicated widely different features of the NEXAFS spectra compared to the neutral species. In addition, some of the core-excited states of the ion correspond to states reached in core-level photoemission of the neutral molecule. In the ionic NEXAFS the final states are, however, reached from a different initial state, and the interpretation of the spectra is simplified due to the dipole selectivity. This facilitates a detailed characterization of several core-excited states that were earlier hidden in the photoemission background. The bare core-hole state, as well as states with several open shells and different spin coupling, can be investigated in detail, and strongly correlated states are identified in long irregular progressions of spectral features [5,6,8]. Although isoelectronic, the spectral signatures come out very differently for the two N_2^+ and CO^+ molecules, and in the case of CO^+, also quite distinct for the two core-hole sites.

Here we explore this method [11] to measure NEXAFS spectra of molecular ions further by presenting the oxygen and nitrogen K edges of the nitrosonium ion (NO^+), which represents a case of a closed-shell cation created from an open-shell species. We show that this indeed leads to the simplicity of closed-shell NEXAFS, while differences from the spectra of the neutral form is present due to the stronger Coulomb potential experienced by the electrons. As NO^+ is isoelectronic with the closed-shell systems N_2 and N_2H^+, and the coupling between the electrons is expected to be qualitatively similar, we will also provide a comparison between the three species. We focus on the formation of the spectra in terms of valence transitions, of Rydberg series, of σ^*, and continuum resonances. The results from the three computational approaches are analyzed; the static exchange method [12],

*rebecka.lindblad@physics.uu.se
†rcc@kth.se

implementing the independent particle approximation in the limit of a close to complete one-particle basis set; the electron-correlated active space (RASSCF [13–15]) and active space perturbation theory (RASPT2 [16]) methods. Experimental and theoretical details, results, discussions, and concluding remarks are presented in the following.

II. EXPERIMENT

NEXAFS in ion yield of the NO^+ molecular cation was measured at the UE52-PGM beamline at BESSY II using the Ion Trap end-station [5,11]. The central part of this experimental station is a linear radio frequency ion trap cooled to cryogenic temperatures. NO was ionized in a He plasma created by a magnetron sputter source. The molecular ions NO^+ were selected by a quadrupole mass filter and further guided to the trap, which is aligned with the x-ray beam. After x-ray absorption, the core-excited states relax mainly via Auger decay after which the molecular ions dissociate. The fragment ions N^+ and O^+ were also stored in the trap and detected with a reflectron time-of-flight mass spectrometer. Action spectra of NO^+, assumed to be proportional to the x-ray absorption spectrum, were produced by monitoring the fragment yield while scanning the photon energy. The different fragments gave very similar ion yield spectra.

Ion yield spectra of the full energy range from the lowest (π^*) resonance to above the ionization potentials were measured for the nitrogen K edge with a step size of 35 meV and a resolution of 112 meV. For the oxygen K edge the step size was 100 meV and the resolution 120 meV. High resolution measurements of the π^* resonances were performed using a step size of 15 meV for nitrogen and 25 meV for oxygen, in both cases with a resolution of 60 meV. Before the measurements, the beamline was calibrated using the neon $1s$-$3p$ line and different diffraction orders and fix focus constants of the plane grating monochromator (c_{ff} values) [17]. The π^* resonances of neutral N_2 and O_2 were measured in a gas cell with a step size of 8 meV and a resolution of 60 meV and were used to check the photon energy calibration at each edge. The measurement of neutral N_2 also serves as a comparison to the nitrogen edge of NO^+.

Spectroscopic constants of the π^* resonances observed at the nitrogen and oxygen K edges of NO^+ were obtained from a Franck-Condon analysis. The intensity of the transitions were calculated by the Franck-Condon overlap of Morse potential energy curves, and Voigt functions were used to simulate the spectrum. The spectroscopic constants of the excited states were variables in a fit, while the constants of the initial state were fixed and obtained from the literature [18]. The procedure is described in more detail elsewhere [5] and the result of the analysis is shown in Table III.

III. THEORY

Two *ab initio* methods with different characteristics were employed to determine the electronic structure of the core-excited states of the NO^+ cations: the static-exchange (STEX) [12] independent particle approximation and the state-average-restricted active space self-consistent field (RASSCF) [13–15] method. These methods were successfully applied to other molecular ions [5,6,8,19].

TABLE I. Assignment of the NO^+ spectrum at the nitrogen K-edge from MS-RASPT2 calculations together with calculated excitation energy and oscillator strength (f). The energies were shifted by −2. eV in order to match the experiment. The numbers in the first column refer to labels in Fig. 1. For the oscillator strength (f), numerals in square brackets indicate powers of 10.

	Energy (eV)	f (a.u.)	[CI weight (%)] Assignment
1	402.48	1.49[−1]	$[90]2\sigma^{-1}2\pi$
2	412.31	3.90[−3]	$[83]2\sigma^{-1}1\pi^{-1}2\pi^2$
	413.31	2.29[−5]	$[84]2\sigma^{-1}3p\pi$
	414.22	1.16[−5]	$[64]2\sigma^{-1}5\sigma^{-1}2\pi^2$
3	415.21	8.77[−4]	$[87]2\sigma^{-1}1\pi^{-1}2\pi^2$
4	415.8	7.34[−3]	$[17]2\sigma^{-1}3p\sigma/[23]2\sigma^{-1}3s\sigma$
			$[18]2\sigma^{-1}1\pi^{-1}3p\sigma 2\pi$
			$[13]2\sigma^{-1}1\pi^{-1}3s\sigma 2\pi$
5	417.71	3.82[−3]	$[15]2\sigma^{-1}4p\sigma/[16]2\sigma^{-1}3s\sigma$
			$[11]2\sigma^{-1}1\pi^{-1}4p\sigma 2\pi$
			$[14]2\sigma^{-1}1\pi^{-1}3s\sigma 2\pi$
6	418.17	1.69[−2]	$[75]2\sigma^{-1}1\pi^{-1}2\pi^2$
7	419.1	5.84[−3]	$[36]2\sigma^{-1}4\sigma^{-1}2\pi^2$
			$[12]\ 2\sigma^{-1}1\pi^{-1}4p\sigma 2\pi$
8	420.11	1.31[−4]	$[10]2\sigma^{-1}3p\sigma/[20]2\sigma^{-1}4p\sigma$
9	420.24	9.58[−3]	$[82]2\sigma^{-1}4p\pi$
10	421.08	3.82[−2]	$[30]2\sigma^{-1}\sigma^*$
			$[24]2\sigma^{-1}1\pi^{-1}\sigma^*2\pi$
11	421.68	2.16[−3]	$[39]2\sigma^{-1}5p\pi$
			$[26]2\sigma^{-1}1\pi^{-1}2\pi^2$
12	422.79	1.80[−3]	$[44]2\sigma^{-1}5p\pi$
			$[21]2\sigma^{-1}1\pi^{-1}2\pi^2$

The RASSCF calculations were followed by multistate second-order perturbation calculations (MS-RASPT2) [16], as implemented in the OpenMolcas software [20]. The quasistationary core-excited states were optimized by imposing core-valence separation so as to avoid the variational collapse due to filling the core orbital [21,22]. Here, the ANO-RCC-VQZP basis set [23] along with an auxiliary ($8s6p4d$) Rydberg basis set was used. Scalar relativistic effects are included by using a second-order Douglas-Kroll-Hess Hamiltonian [24,25], in combination with the ANO-RCC basis. In the RASPT2 step, an imaginary shift of 0.3 Hartree [26] and the default ionization-potential electron-affinity (IPEA) shift of 0.25 Hartree [27] were in use. The transition dipole moments in the velocity gauge were obtained by the RAS state-interaction approach [28,29].

The MS-RASPT2 spectra presented in Fig. 1 and Tables I and II were computed considering an active space RAS (10,1,3;1,5,20), where the $1s$ orbital is placed in RAS1, the occupied orbitals in RAS2, and unoccupied in RAS3, as previously used [5,6,8]. The RASSCF active space is labeled RAS(n, l, m; i, j, k), where i, j, and k are the number of orbitals in RAS1, RAS2, and RAS3 spaces, respectively, n is the total number of electrons in the active space, l the maximum number of holes allowed in RAS1, and m the maximum number of electrons in RAS3. The theoretical vibrationally resolved spectra shown in Fig. 3 were computed with time-dependent wave-packet formalism [30] with the

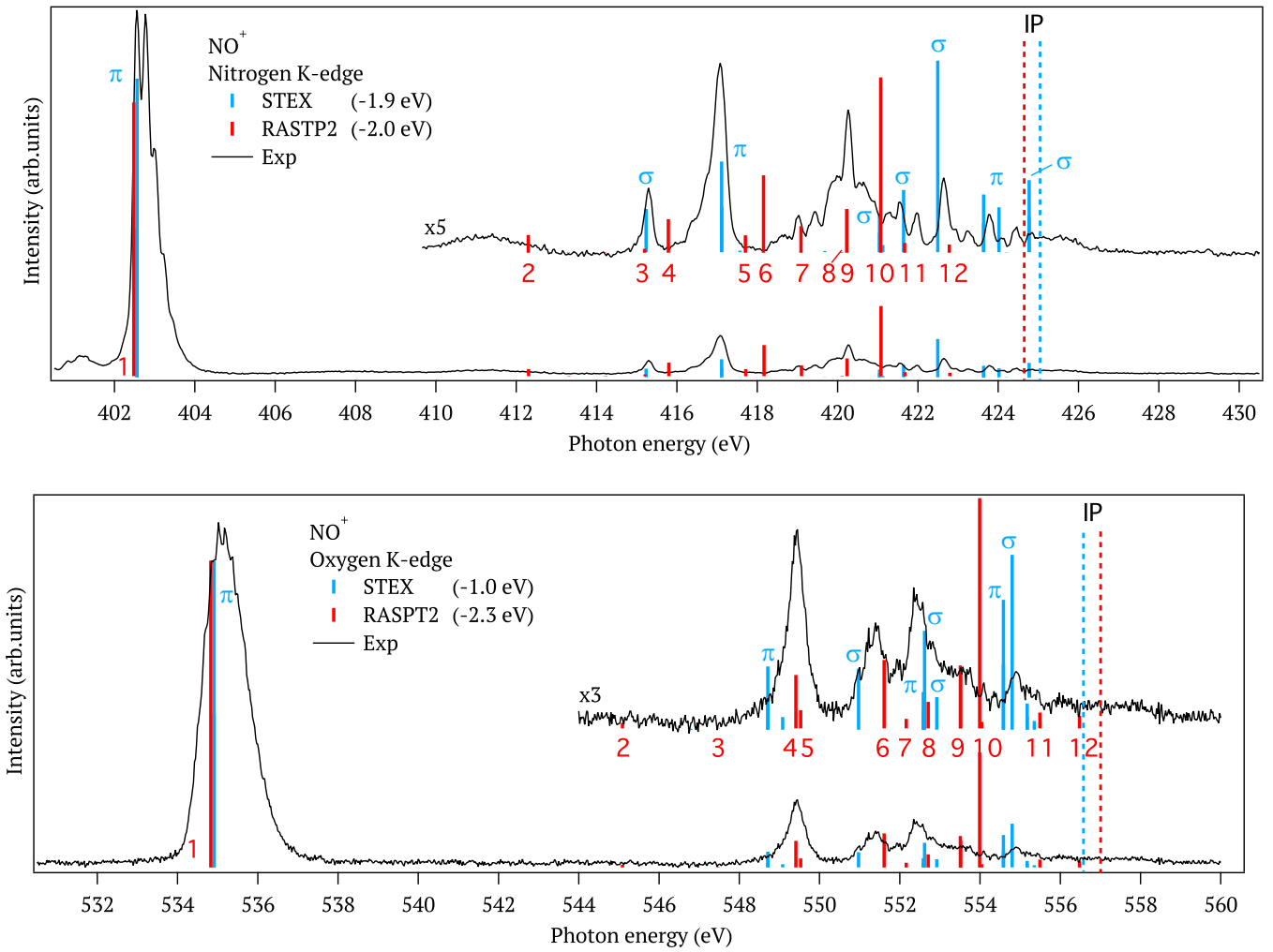

FIG. 1. Experimental and theoretical NEXAFS of NO^+ at nitrogen (top) and oxygen (bottom) K edges. Both STEX (blue) and MS-RASPT2 (red) results at equilibrium geometry are presented and shifted in energy to align with the lowest experimental resonance with the shift reported in the annotation. The dashed vertical lines indicates the theoretical ionization potentials. Calculated MS-RASPT2 transition states are labeled with numbers and their assignments are presented in Tables I and II for N and O K edges, respectively.

ESPEC program [31–33], as described previously [5,6]. The wave packet was propagated on MS-RASPT2 potential energy curves computed with the procedure described above, but with the RAS (10,1,0;1,14,0) active space.

The STEX method does not include electronic correlation but describes the electronic relaxation, and allows for an almost complete basis set to be used thus providing a full one-electron description of the entire spectrum both below the ionization threshold and in the continuum.

IV. RESULTS AND DISCUSSION

A. NO^+ photoabsorption spectra

The N 1s and O 1s NEXAFS spectra of NO^+ are presented in Fig. 1. The two K-edge spectra are very much alike with one strong vibrationally resolved resonance at lower energy (at approximately 403 eV and 535 eV for the nitrogen and oxygen edges, respectively) and, starting from 13 to 15 eV above this, several sharp resonances with lower intensity. This is much different from the corresponding spectra of neutral NO [34,35]. Even though the first strong resonance in both neutral and ionic NO is a result of a $1s \longrightarrow 2\pi$ transition, it is much broader in neutral NO. This is due to the open-shell nature where spin coupling of the electrons in the two singly occupied 2π orbitals to a core electron results in a three-fold multiplet term structure. In NO^+ the single strong 2π (or π^*) resonance resembles instead, in terms of its energetic transition and strong oscillator strength, the π^* resonance in neutral N_2 and CO. The feature seen below 402 eV in Fig. 1 is a result of N_2 contamination, as will be discussed further in Sec. IV B. The NO^+ oxygen 1s spectrum stands out in that the π^* band is much broader with less-resolved vibrational fine-structure. This may be explained by the additive antibonding characters of both π^* and O 1s orbitals leading to longer bond length and eventually a fully repulsive potential [36]. Just as for the N_2 and CO molecules, the strong π^* intensity for NO^+ (N and O spectra) depletes, by virtue of the oscillator strength sum rule, the intensity of the other peaks. A second noticeable difference, with respect to neutral NO and also N_2 and CO, is that the range of narrow resonances is much wider: the energy difference from π^* to the core ionization potential (IP) in the two spectra roughly doubles that of the neutral species. This

TABLE II. Assignment of the NO^+ spectrum at the oxygen K-edge from MS-RASPT2 calculations together with calculated excitation energy and oscillator strength (f). The energies were shifted by −2.3 eV in order to match the experiment. Numbers in the first column refer to labels in Fig. 1. For the oscillator strength (f), numerals in square brackets indicate powers of 10.

	Energy (eV)	f(a.u.)	[CI weight (%)] Assignment
1	534.80	9.63[−2]	$[65]1\sigma^{-1}2\pi$
2	545.06	8.52[−4]	$[75]\ 1\sigma^{-1}5\sigma^{-1}2\pi^2$
3	547.44	5.24[−5]	$[46]1\sigma^{-1}3s\sigma/[26]1\sigma^{-1}3p\sigma$
4	549.38	8.35[−3]	$[82]1\sigma^{-1}1\pi^{-1}2\pi^2$
5	549.5	2.82[−3]	$[43]1\sigma^{-1}3p\sigma/[25]1\sigma^{-1}3s\sigma$
6	551.58	1.07[−2]	$[67]1\sigma^{-1}3p\sigma$
			$[20]1\sigma^{-1}1\pi^{-1}2\pi 3p\sigma$
7	552.13	1.48[−3]	$[48]1\sigma^{-1}3p\pi$
			$[30]1\sigma^{-1}1\pi^{-1}2\pi 3p\pi$
8	552.68	4.15[−3]	$[45]1\sigma^{-1}1\pi^{-1}2\pi^2$
9	553.48	9.85[−3]	$[51]1\sigma^{-1}4p\pi$
			$[34]1\sigma^{-1}1\pi^{-1}2\pi 4p\pi$
9	553.49	8.45[−3]	$[54]1\sigma^{-1}4s\sigma/[17]1\sigma^{-1}\sigma^*$
10	553.96	3.61[−2]	$[49]1\sigma^{-1}\sigma^*/[17]1\sigma^{-1}4s\sigma$
10	554.01	1.02[−3]	$[51]1\sigma^{-1}5p\pi$
			$[37]1\sigma^{-1}1\pi^{-1}2\pi 5p\pi$
11	555.46	2.45[−3]	$[73]1\sigma^{-1}1\pi^{-1}2\pi^2$
12	556.45	1.93[−3]	$[62]1\sigma^{-1}4\sigma^{-1}2\pi^2$

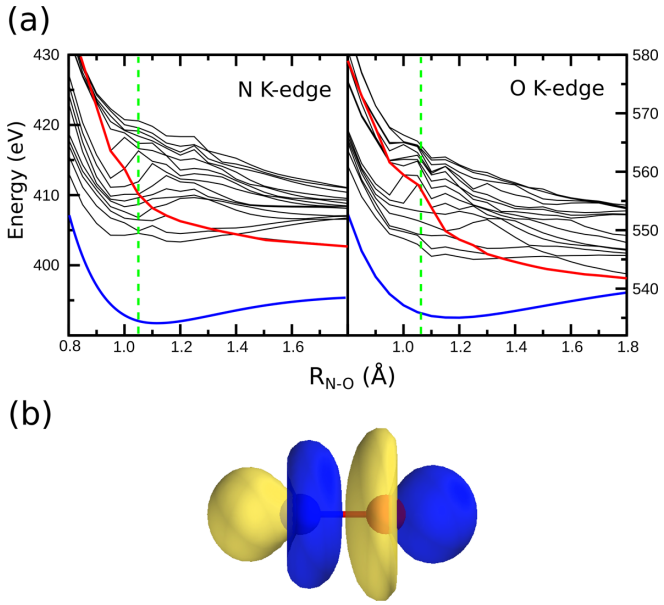

FIG. 2. (a) MS-RASPT2 potential energy curves of NO^+ at nitrogen (left) and oxygen (right) K edges. The black curves are the potentials of a_1 symmetry (considering the $C_{\infty h}$ point group), with red curve highlighting the potential related to the σ^* transition. The blue curve represents the π^* (from b_1 symmetry) potential and the dashed green line shows the Franck-Condon position. (b) MS-RASPT2 natural molecular orbital σ^* of NO^+.

is accompanied by an integral intensity shift in both spectra to the upper sharp resonances (below IP), with the first ca 10 eV range from the π^* excitation that is devoid of intensity. The strong dication (core-hole + valence-hole) potential compared to the single core-hole potential is the obvious cause for this effect. It leaves a quite irregular remainder of sharp resonances of σ and π transitions (see assignment in Tables I and II). A closer look at the NO^+ MS-RASPT2 spectra shows that the single excitation ns and np series of transitions can be discerned in both spectra calculated by MS-RASPT2; however, for most states a rather significant configuration mixing is predicted by this method.

Another salient and perhaps the most conspicuous difference between the NEXAFS spectra of neutral and ionized NO^+ is the position of the σ^* resonance. While being observed in the continuum of the neutral species, it is now found in the discrete spectral part of the ionic NO^+, at 420 eV and 553 eV (421.1 and 554.0 eV in the MS-RASPT2 calculations, see Tables I and II) in the nitrogen and oxygen spectra, respectively. This is a further effect of the more attractive potential in NO^+. In the vertical calculation at the ground-state equilibrium geometry, the σ^* transition is predicted to be relatively strong in both spectra (and in both types of calculations) at variance with its experimental appearance. The reason for this discrepancy is seen in the potential energy plot in Fig. 2(a) – showing that the σ^* core state is strongly dissociative, something we can derive from the antibonding character of the σ^* orbital [see Fig. 2(b)]. It can be relevant to compare with the normal case of the σ^* shape resonance in the continuum of several diatomic molecules, where the excited electron is temporarily "trapped" by a potential barrier which dictates its localization and coupling to the electron continuum. Thus, roughly speaking, in the neutral NO (like many other diatomics) the broadening of the σ^* transitions is caused by double coupling to nuclear and electronic continua, while this is changed to mainly nuclear continuum broadening when, in the cation, the increased positive charge moves the core $\longrightarrow \sigma^*$ transition below the ionization potential. This coupling (see Fig. 2) though is strong enough and, when

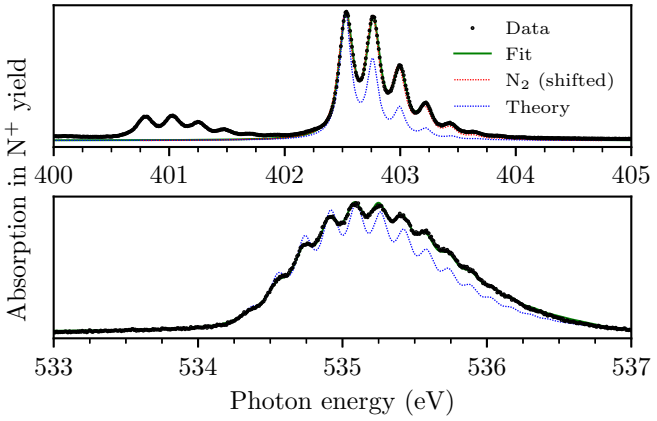

FIG. 3. High-resolution experimental spectra of the nitrogen K edge (top) and oxygen K edge (bottom) π^* resonances of NO^+. The fitted parameters are given in Table III. On the nitrogen edge we observe contamination of N_2 in the photon energy region 400.7–402.0. A comparison to the XAS spectrum of neutral N_2, shifted by +1.75 eV, is shown in dashed red and overlaps completely with NO^+. Theoretical MS-RASPT2 spectra are shifted +0.12 eV at the nitrogen K edge and +1.98 eV at the oxygen K edge.

TABLE III. Spectroscopic constants from Franck-Condon fits of the experimental oxygen and nitrogen K-edge spectra of NO^+ (top) and from theoretical MS-RASPT2 spectra (bottom). E_{00} is the energy difference between the lowest vibrational level in the ground state and the lowest vibrational level in the excited state, ω_e and $\omega_e\chi_e$ are the first and second vibrational constants, and ΔR_e is the shift in internuclear equilibrium distance. γ is the Lorentzian broadening given as FWHM. The experimental equilibrium bond length for the ionic ground state is 1.06325 Å [18]. The uncertainties of the fitted model were estimated using Markov chain Monte Carlo [44,45]. The uncertainty of E_{00} is dominated by the photon bandwidth.

State	E_{00} (eV)	ω_e (meV)	$\omega_e\chi_e$ (meV)	ΔR_e (Å)	γ (meV)
Experiment					
Ground	–	294.68 [18]	2.0 [18]	–	
$2\sigma^{-1}2\pi$	402.53	242.3 ± 1.6	3.1 ± 0.5	$+0.06 \pm 0.005$	130 ± 5
$1\sigma^{-1}2\pi$	534.36	190.3 ± 0.3	2.0 ± 0.1	$+0.14 \pm 0.005$	–
Theory					R_e (Å)
Ground	–	290.64	1.97	–	1.067
$2\sigma^{-1}2\pi$	402.43	244.63	3.04	+0.05	1.117
$1\sigma^{-1}2\pi$	532.43	195.13	2.60	+0.13	1.199

included in the model, it significantly broadens the σ^* band shape by many eVs, making the theoretical and experimental spectra agree better in this energy range. Some of the upper lying core-excited states potentials also show a dissociative character (Fig. 2), however, the σ^* presents the most striking effect. A more precise determination of the appearance of the σ^* and of the interacting close-lying remainder states calls for high-resolution measurements of this energy region compared to calculations using a high-level multistate nuclear dynamics approach with nonadiabatic coupling. This is beyond the scope of the present paper, but we can still highlight the similarity of the situation of the coupling of a dissociative σ^* with a set of discrete Rydberg states as it appears in the NEXAFS spectrum of neutral O_2 [37–40].

Comparing the overall spectral RASPT2 and STEX results we see that the later results miss, as expected, the transitions with strong multielectron character predicted by RASPT2, while we can find correspondence between the two approaches concerning one-particle-dominant transitions although with somewhat altered intensities and energy positions. In particular, the σ^* transition comes out very strongly in the two types of calculations. The STEX calculations tend to widen the spectra with more oscillator strength towards higher energies.

B. Vibrational analysis

The main π^* resonances are vibrationally resolved at both the nitrogen and oxygen K edges (see Fig. 3), allowing determination of the spectroscopic constants for the core excited states, see Table III. The same $1\sigma^{-1}2\pi$ (O $1s^{-1}$) and $2\sigma^{-1}2\pi$ (N $1s^{-1}$) configurations are reached in core-level photoemission of neutral NO. The vibrational progression of the N $1s^{-1}$ states in x-ray photoelectron spectroscopy (XPS) gives an internuclear equilibrium distance of 1.13 Å [41], which is close to the distance obtained here. Adding our experimental shift in equilibrium distance +0.06 Å (see Table III), to the ionic ground-state equilibrium distance 1.06325 Å [18], we get 1.13 Å. However, our harmonic vibrational energy ($\omega_e = 242$ meV) is higher than the value 228 meV obtained in XPS [41]. A difference between photoemission of the neutral molecule and XAS of the ion is that dipole selectivity ensures that only the singlet final state is populated in XAS. Additional broadening due to the Doppler effect or asymmetry caused by postcollision interaction may also hamper the line-shape analysis in photoemission. In addition, the $^2\Pi_{3/2}$ and $^2\Pi_{1/2}$ initial states of the neutral molecule are split by 15 meV [42], and both contribute to the spectra in room temperature experiments.

At the nitrogen K edge we observe contamination of N_2 in the photon energy region 400.7–402.0 eV, which enables us a precise energy calibration. We note that the vibrational profile associated with the $2\sigma^{-1}2\pi$ excitation almost coincides with the $1\sigma_u^{-1}1\pi_g$ of N_2 if the latter is shifted +1.75 eV. The excitations are similar as both systems go from a closed-shell ground state to a state with a nitrogen core vacancy and an electron in the first anti-bonding π orbital. The observation suggests that the potential-surface change induced by the excitation is little affected by "inside protonation", i.e., by the change of the charge of the neighboring nucleus. The agreement between the two spectra may be surprising in view of the differing equilibrium bond lengths of the ground states of N_2 (1.098 Å) and NO^+ (1.063 Å).

The detailed analysis of the profile gives a Lorentzian width of full width at half maximum (FWHM) = 130 meV for the π^* resonance in NO^+, suggesting a slightly shorter lifetime than the corresponding state in N_2 where FWHM = 115 meV [43]. The theoretical spectra are in good agreement with the experimental vibrational progressions (Fig. 3), and the derived optical constants are close to the experimental ones (Table III).

C. Comparison with NEXAFS spectra of isoelectronic nitrogen containing species

The spectra of the isoelectronic species N_2, N_2H^+, NO^+(N), and NO^+(O) show similarities but also some salient differences, see Fig. 4. They all share the feature of a very strong oscillator strength to the first antibonding valence π^* orbital, exhibiting quite similar vibrational progressions between the species, followed by weak irregular high-energy excitations, being different from pure Rydberg progressions.

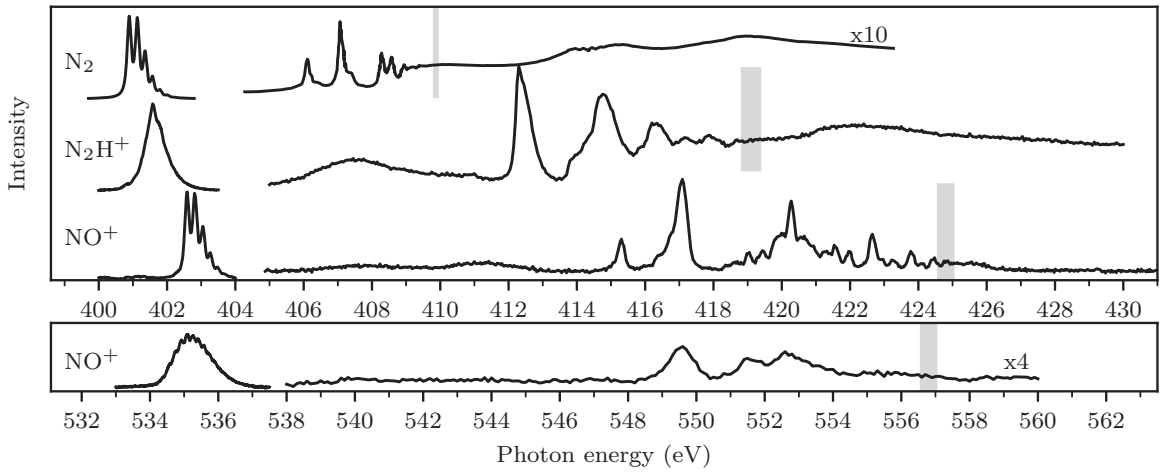

FIG. 4. The experimental x-ray absorption spectrum of N_2, N_2H^+, and NO^+ at the nitrogen K edge and for NO^+ also at the oxygen K edge. The higher-energy parts are enlarged by a factor of 10 at the nitrogen K edge and a factor of 4 at the oxygen K edge. The high-energy part of the N_2 spectrum is adapted from Ref. [46]. The estimated ionization potentials are indicated by gray lines [8,47].

The effect of protonation is primarily to extend the spectra, in case of "internal protonation" [NO^+(N) and NO^+(O)] the distance from the π^* band to the ionization potential is roughly doubled with respect to N_2, while for "external protonation" (N_2H^+) the extension is given by a factor of 1.5. Two other salient differences can be highlighted, namely, the emergence of the distance dependent low-energy charge transfer peak in case of N_2H^+ [8], and the discrete character of the σ^* excitation in cases of NO^+(N) and NO^+(O).

For the well-known NEXAFS spectrum of N_2 the dominating excitations from the nitrogen core level to the lowest unoccupied orbital (LUMO), π^*, i.e., the $1\sigma_u^{-1}1\pi_g$ excitation, occurs around 401 eV. At higher energies the Rydberg-like series converge to the ionization thresholds around 410 eV, followed by double excitations and a shape resonance in the 412 to 420 range [46]. To emphasize details, this part of the spectrum in Fig. 4 is multiplied by a factor of 10 compared the π^* resonance. As noted, the general appearance of the NEXAFS spectra of the N_2H^+ and NO^+ cations are strikingly similar to the N_2 spectrum. They are dominated by the π^* resonance, only slightly shifted towards higher energies. The vibrational fine-structure in this resonance is modified in the N_2H^+ spectrum, but reappears in NO^+ where the fine-structure is almost identical to the N_2 fine-structure. The features at higher energies show a complex pattern below the ionization limits, which are estimated to be around 419 eV for N_2H^+ and 425 eV for NO^+. The higher-energy features, also here multiplied by a factor of 10, are more intense, relative to the π^* resonance than in the N_2 spectrum, and the trend is that the sharp spectral structures shift to higher energies with the ionization limits.

In the case of N_2H^+ (we refer to Ref. [8] for a detailed analysis) the separation of the two π^* peaks and the evolution of the electronic structure and of the charge transfer excitation show smooth dependence on the proton position. There is a clear extension of the spectra going from infinite distance of the proton to the compound nucleus where fine-structures show some, although not fully detailed, similarities. An interesting feature of partial localization of the nitrogen core orbitals with respect to proton distance could be unraveled in Ref. [8]. This localization shows a strong, nonmonotonous variation with proton distance qualitatively independent of the theory method applied.

Concerning the remaining part of the spectrum we disclosed that cationic spectra [N_2H^+, NO^+(N) and NO^+(O)] also show a complicated non-Rydberg structure. The wide high-energy part of the spectra exhibit some detailed and irregular structures for which a one-to-one mapping between orbitals and states cannot be made. It displays rather that the molecular orbital picture in some parts breaks down and is replaced by a situation where Rydberg one-electron and two-electron two-hole transitions coexist. The role of electron correlation, as predicted by RASSCF calculations, is thus significant; something also observed in isoelectronic N_2H^+ species, and even more prevalent in the cases of N_2^+ and CO^+, where the so-called semi-internal configuration interaction can be identified [5,6].

V. SUMMARY

In this paper we presented results from continuing efforts to measure and characterize NEXAFS spectra from molecular cationic species. Thus, earlier studies of N_2^+ [5], CO^+ [6], and N_2H^+ [8] cations that indicated features of the spectra widely different from those of closed-shell species are here complemented by NO^+ at the nitrogen and oxygen edges. Salient differences from the NEXAFS spectra of NO, and also of the well attended N_2 and CO spectra, could be unravelled; in particular a doubling of the full spectral width from the first resonance to the ionization potential, a depletion of intensity in a large interval above the π^* resonance, and an energy shift of the strongly repulsive σ^* resonance from the continuum to below the ionization potential. Higher up in the spectra complicated non-Rydberg structures appear for which the molecular orbital picture in some parts breaks down and is replaced by a situation where Rydberg one-electron and two-electron two-hole transitions coexist.

A comparison with NEXAFS spectra of isoelectronic nitrogen containing species N_2, N_2H^+, NO^+(N), and NO^+(O) was made. Similarities and convergent trends between the

discrete parts of the spectra could be discerned, apart from the additional charge transfer transition to the proton in the N_2H^+ case.

ACKNOWLEDGMENTS

Beamtime for this project was granted at the Ion Trap endstation at BESSY II beamline UE52-PGM, operated by Helmholtz-Zentrum Berlin. The computations were enabled by resources provided by the Swedish National Infrastructure for Computing (SNIC) at the High Performance Computing Center North (HPC2N) partially funded by the Swedish Research Council through Grant Agreement No. SNIC 2021/3-22. This project received funding from the European Union's Horizon 2020 research and innovation program under Grant Agreement No. 730872 and by the German Federal Ministry of Education and Research (BMBF) through Grant No. BMBF-05K16Vf2. R.L. and J.-E.R. acknowledge funding from the Swedish Research Council, Contracts No. 637-2014-6929 and No. 2014-04518, respectively.

[1] J.-P. Mosnier, E. T. Kennedy, P. van Kampen, D. Cubaynes, S. Guilbaud, N. Sisourat, A. Puglisi, S. Carniato, and J.-M. Bizau, Inner-shell photoexcitations as probes of the molecular ions CH^+, OH^+, and SiH^+: Measurements and theory, Phys. Rev. A **93**, 061401(R) (2016).

[2] S. Klumpp, A. A. Guda, K. Schubert, K. Mertens, J. Hellhund, A. Müller, S. Schippers, S. Bari, and M. Martins, Photoabsorption of the molecular IH cation at the iodine 3*d* absorption edge, Phys. Rev. A **97**, 033401 (2018).

[3] S. Bari, L. Inhester, K. Schubert, K. Mertens, J. O. Schunck, S. Dörner, S. Deinert, L. Schwob, S. Schippers, A. Müller, S. Klumpp, and M. Martins, Inner-shell x-ray absorption spectra of the cationic series NHy+ (y = 0–3), Phys. Chem. Chem. Phys. **21**, 16505 (2019).

[4] K. Schubert, A. A. Guda, K. Mertens, J. O. Schunck, S. Schippers, A. Müller, S. Bari, S. Klumpp, and M. Martins, Absorption spectra at the iodine 3d ionisation threshold following the CHxI+ (x = 0–3) cation sequence, Phys. Chem. Chem. Phys. **21**, 25415 (2019).

[5] R. Lindblad, L. Kjellsson, R. C. Couto, M. Timm, C. Bülow, V. Zamudio-Bayer, M. Lundberg, B. von Issendorff, J. T. Lau, S. L. Sorensen, V. Carravetta, H. Ågren, and J.-E. Rubensson, X-Ray Absorption Spectrum of the N_2^+ Molecular Ion, Phys. Rev. Lett. **124**, 203001 (2020).

[6] R. C. Couto, L. Kjellsson, H. Ågren, V. Carravetta, S. L. Sorensen, M. Kubin, C. Bülow, M. Timm, V. Zamudio-Bayer, B. von Issendorff, J. T. Lau, J. Söderström, J.-E. Rubensson, and R. Lindblad, The carbon and oxygen k-edge nexafs spectra of CO^+, Phys. Chem. Chem. Phys. **22**, 16215 (2020).

[7] S. Carniato, J.-M. Bizau, D. Cubaynes, E. T. Kennedy, S. Guilbaud, E. Sokell, B. McLaughlin, and J.-P. Mosnier, Vibrationally and spin-orbit-resolved inner-shell x-ray absorption spectroscopy of the NH^+ molecular ion: Measurements and ab initio calculations, Atoms **8**, 67 (2020).

[8] R. C. Couto, W. Hua, R. Lindblad, L. Kjellsson, S. L. Sorensen, M. Kubin, C. Bülow, M. Timm, V. Zamudio-Bayer, B. Von Issendorff, J. Söderström, J. T. Lau, J.-E. Rubensson, H. Ågren, and V. Carravetta, Breaking inversion symmetry by protonation: Experimental and theoretical nexafs study of the diazynium ion, $N2H^+$, Phys. Chem. Chem. Phys. **23**, 17166 (2021).

[9] M. Martins, S. Reinwardt, J. O. Schunck, J. Schwarz, K. Baev, A. Müller, T. Buhr, A. Perry-Sassmannshausen, S. Klumpp, and S. Schippers, Disentangling the photodissociation dynamics of the HF^+ molecular radical via kinetic-energy-release-resolved F 1s core excitation and ionization, J. Phys. Chem. Lett. **12**, 1390 (2021).

[10] E. T. Kennedy, Interaction of short wavelength photons with atomic and molecular ions: 50 years some examples, Phys. Scr. **97**, 054003 (2022).

[11] K. Hirsch, J. T. Lau, P. Klar, A. Langenberg, J. Probst, J. Rittmann, M. Vogel, V. Zamudio-Bayer, T. Möller, and B. von Issendorff, X-ray spectroscopy on size-selected clusters in an ion trap: From the molecular limit to bulk properties, J. Phys. B: At., Mol. Opt. Phys. **42**, 154029 (2009).

[12] H. Ågren, V. Carravetta, O. Vahtras, and L. G. Pettersson, Direct SCF direct static-exchange calculations of electronic spectra, Theor. Chem. Acc. **97**, 14 (1997).

[13] H. J. A. Jensen, P. Jørgensen, and H. Ågren, Efficient optimization of large scale MCSCF wave functions with a restricted step algorithm, J. Chem. Phys. **87**, 451 (1987).

[14] P. Å. Malmqvist, A. Rendell, and B. O. Roos, The restricted active space self-consistent-field method, implemented with a split graph unitary group approach, J. Phys. Chem. **94**, 5477 (1990).

[15] H. Ågren, A. Flores-Riveros, and H. Jensen, An efficient method for calculating molecular radiative intensities in the VUV and soft x-ray wavelength regions, Phys. Scr. **40**, 745 (1989).

[16] P. Å. Malmqvist, K. Pierloot, A. R. M. Shahi, C. J. Cramer, and L. Gagliardi, The restricted active space followed by second-order perturbation theory method: Theory and application to the study of CuO_2 and Cu_2O_2 systems, J. Chem. Phys. **128**, 204109 (2008).

[17] M. R. Weiss, R. Follath, K. J. S. Sawhney, and T. Zeschke, Absolute energy calibration for plane grating monochromators, Nucl. Instrum. Methods Phys. Res. A: Accel. Spectrom. Detect. Assoc. Equip. **467-468**, 482 (2001).

[18] D. L. Albritton, A. L. Schmeltekopf, and R. N. Zare, Potential energy curves for NO^+, J. Chem. Phys. **71**, 3271 (1979).

[19] V. Carravetta, R. C. Couto, and H. Ågren, X-ray absorption of molecular cations—a new challenge for electronic structure theory, J. Phys.: Condens. Matter **34**, 363002 (2022).

[20] I. Fdez. Galván, M. Vacher, A. Alavi, C. Angeli, F. Aquilante, J. Autschbach, J. J. Bao, S. I. Bokarev, N. A. Bogdanov, R. K. Carlson *et al.*, Openmolcas: From source code to insight, J. Chem. Theory Comput. **15**, 5925 (2019).

[21] L. S. Cederbaum, W. Domcke, and J. Schirmer, Many-body theory of core holes, Phys. Rev. A **22**, 206 (1980).

[22] M. G. Delcey, L. K. Sørensen, M. Vacher, R. C. Couto, and M. Lundberg, Efficient calculations of a large number of highly excited states for multiconfigurational wavefunctions, J. Comput. Chem. **40**, 1789 (2019).

[23] B. O. Roos, R. Lindh, P.-Å. Malmqvist, V. Veryazov, and P.-O. Widmark, Main group atoms and dimers studied with a new relativistic ano basis set, J. Phys. Chem. A **108**, 2851 (2004).

[24] M. Douglas and N. M. Kroll, Quantum electrodynamical corrections to the fine structure of helium, Ann. Phys. (NY) **82**, 89 (1974).

[25] B. A. Hess, Relativistic electronic-structure calculations employing a two-component no-pair formalism with external-field projection operators, Phys. Rev. A **33**, 3742 (1986).

[26] N. Forsberg and P.-Å. Malmqvist, Multiconfiguration perturbation theory with imaginary level shift, Chem. Phys. Lett. **274**, 196 (1997).

[27] G. Ghigo, B. O. Roos, and P.-Å. Malmqvist, A modified definition of the zeroth-order hamiltonian in multiconfigurational perturbation theory (CASPT2), Chem. Phys. Lett. **396**, 142 (2004).

[28] P.-Å. Malmqvist and B. O. Roos, The CASSCF state interaction method, Chem. Phys. Lett. **155**, 189 (1989).

[29] P. Å. Malmqvist, B. O. Roos, and B. Schimmelpfennig, The restricted active space (RAS) state interaction approach with spin–orbit coupling, Chem. Phys. Lett. **357**, 230 (2002).

[30] F. Gel'mukhanov and H. Ågren, Resonant x-ray raman scattering, Phys. Rep. **312**, 87 (1999).

[31] V. C. Felicíssimo, F. F. Guimarães, F. Gel'mukhanov, A. Cesar, and H. Ågren, The principles of infrared-x-ray pump-probe spectroscopy. Applications on proton transfer in core-ionized water dimers, J. Chem. Phys. **122**, 094319 (2005).

[32] R. C. Couto, V. V. Cruz, E. Ertan, S. Eckert, M. Fondell, M. Dantz, B. Kennedy, T. Schmitt, A. Pietzsch, F. F. Guimarães, H. Ågren, F. Gel'mukhanov, M. Odelius, V. Kimberg, and A. Föhlisch, Selective gating to vibrational modes through resonant x-ray scattering, Nat. Commun. **8**, 14165 (2017).

[33] V. Vaz da Cruz, E. Ertan, R. C. Couto, S. Eckert, M. Fondell, M. Dantz, B. Kennedy, T. Schmitt, A. Pietzsch, F. F. Guimarães, H. Ågren, F. Gel'mukhanov, M. Odelius, A. Föhlisch, and V. Kimberg, A study of the water molecule using frequency control over nuclear dynamics in resonant x-ray scattering, Phys. Chem. Chem. Phys. **19**, 19573 (2017).

[34] R. Püttner, I. Dominguez, T. J. Morgan, C. Cisneros, R. F. Fink, E. Rotenberg, T. Warwick, M. Domke, G. Kaindl, and A. S. Schlachter, Vibrationally resolved O 1*s* core-excitation spectra of CO and NO, Phys. Rev. A **59**, 3415 (1999).

[35] A. Ehresmann, W. Kielich, L. Werner, P. V. Demekhin, D. V. Omel'yanenko, V. L. Sukhorukov, K.-H. Schartner, and H. Schmoranzer, Lifetime vibrational interference during the NO 1s-1π* resonant excitation studied by the NO+(A $^1\Pi$ – X $^1\Sigma^+$) fluorescence, Eur. Phys. J. D **45**, 235 (2007).

[36] J. Müller and H. Ågren, Role of core hole state geometry in molecular electron spectroscopies, in *Molecular Ions: Geometric and Electronic Structures*, edited by J. Berkowitz and K.-O. E. Groeneveld (Springer, Boston, 1983), pp. 221–270.

[37] P. Baltzer, M. Larsson, L. Karlsson, B. Wannberg, and M. Carlsson Göthe, Inner-valence states of $N2^+$ studied by UV photoelectron spectroscopy and configuration-interaction calculations, Phys. Rev. A **46**, 5545 (1992).

[38] J.-I. Adachi, N. Kosugi, and A. Yagishita, Symmetry-resolved soft x-ray absorption spectroscopy: Its application to simple molecules, J. Phys. B: At., Mol. Opt. Phys. **38**, R127 (2005).

[39] S. L. Sorensen, K. J. Børve, R. Feifel, A. de Fanis, and K. Ueda, The O 1s photoelectron spectrum of molecular oxygen revisited, J. Phys. B: At., Mol. Opt. Phys. **41**, 095101 (2008).

[40] R. Püttner and K. Ueda, The angularly resolved O 1s ion-yield spectrum of O2 revisited, J. Chem. Phys. **145**, 224302 (2016).

[41] M. Hoshino, R. Montuoro, R. R. Lucchese, A. D. Fanis, U. Hergenhahn, G. Prümper, T. Tanaka, H. Tanaka, and K. Ueda, Vibrationally resolved partial cross sections and asymmetry parameters for nitrogen k-shell photoionization of the NO molecule, J. Phys. B: At., Mol. Opt. Phys. **41**, 085105 (2008).

[42] A. Malakhovskii and A. Gedanken, Stern–Gerlach study of nitric oxide, J. Chem. Soc., Faraday Trans. **92**, 329 (1996).

[43] K. C. Prince, L. Avaldi, M. Coreno, R. Camilloni, and M. de Simone, Vibrational structure of core to Rydberg state excitations of carbon dioxide and dinitrogen oxide, J. Phys. B: At., Mol. Opt. Phys. **32**, 2551 (1999).

[44] M. Newville, T. Stensitzki, D. B. Allen, and A. Ingargiola, LMFIT: Non-Linear Least-Square Minimization and Curve-Fitting for Python, Zenodo (2014), https://doi.org/10.5281/zenodo.11813.

[45] D. Foreman-Mackey, D. W. Hogg, D. Lang, and J. Goodman, emcee: The MCMC hammer, Publ. Astron. Soc. Pac. **125**, 306 (2013).

[46] C. T. Chen, Y. Ma, and F. Sette, K-shell photoabsorption of the N_2 molecule, Phys. Rev. A **40**, 6737 (1989).

[47] M. Alagia, R. Richter, S. Stranges, M. Agåker, M. Ström, J. Söderström, C. Såthe, R. Feifel, S. Sörensen, A. De Fanis, K. Ueda, R. Fink, and J.-E. Rubensson, Core level ionization dynamics in small molecules studied by x-ray-emission threshold-electron coincidence spectroscopy, Phys. Rev. A **71**, 012506 (2005).